Materials Today Chemistry 29 (2023) 101474

Contents lists available at ScienceDirect

Materials Today Chemistry

journal homepage: www.journals.elsevier.com/materials-today-chemistry/

A first-principles study of self-healing binders for next-generation Si-based lithium-ion batteries

R. Maji [a, *], M.A. Salvador [b], A. Ruini [b, d, e], R. Magri [b, d, e], E. Degoli [c, d, e]

[a] Dipartimento di Scienze e Metodi Dell'Ingegneria, Università di Modena e Reggio Emilia, Via Amendola 2 Padiglione Tamburini, I-42122, Reggio Emilia, Italy
[b] Dipartimento di Scienze Fisiche, Informatiche e Matematiche Sede Ex-Fisica, Università di Modena e Reggio Emilia, Via Campi 213/A, 41125 Modena, Italy
[c] Dipartimento di Scienze e Metodi Dell'Ingegneria, Università di Modena e Reggio Emilia and Centro Interdipartimentale En&Tech, Via Amendola 2 Padiglione Morselli, I-42122 Reggio Emilia, Italy
[d] Centro S3, Istituto Nanoscienze-Consiglio Nazionale Delle Ricerche (CNR-NANO), Via Campi 213/A, 41125 Modena, Italy
[e] Centro Interdipartimentale di Ricerca e per I Servizi Nel Settore Della Produzione, Stoccaggio Ed Utilizzo Dell'Idrogeno H2-MO.RE., Via Università 4, 41121 Modena, Italy

ARTICLE INFO

Article history:
Received 27 September 2022
Received in revised form
27 January 2023
Accepted 24 February 2023
Available online 22 March 2023

Keywords:
Si anodes
PVA
PANI
Boronic-acid group
DFT
Li-ion batteries

ABSTRACT

Silicon anodes typically suffer from poor intrinsic conductivity and dramatic volume change during charge/discharge cycles, which hinders their commercialization in high energy density lithium-ion batteries (LiBs). This issue can be alleviated by embedding particles of the active material in an adhesive matrix, such as a polymer binder, that can accommodate large volume changes during lithiation and delithiation. Several research efforts have aimed at enhancing the adhesive, elastic, electrical, and ionic properties of binders for use in silicon anodes. Therefore, stable silicon/polymer interfaces are crucial for the performance of high capacity silicon-based LiBs. In this research, we focused on the definition of the mechanisms that determine the adhesion properties of a couple of recently proposed self-healing polymers, on Si-surfaces. The structural and electronic properties as well as the energetics of boronic acid-doped polyaniline and polyvinyl alcohol monomers absorbed on Si (110) and Si (111) surfaces have been investigated through first-principles calculations based on the density functional theory. We showed that the coabsorption of these two monomers increases the absorption energy and in general improves the adhesion properties of both polymers on both Si-surfaces, especially on the Si (111) facet.

1. Introduction

Rechargeable Li-ion batteries (LIBs) are widely used today as electrochemical energy storage devices in consumer electronics, smart grids, and electric vehicles because of their high energy density and long life cycle. Although graphite holds the main market of anodic materials in commercial LIBs due to its cycling stability, the observed low theoretical capacity (372 mAh/g, LiC_6) hinders its further development for high-energy LIBs [1]. Silicon is the most promising anode material for next-generation high-energy-density LIBs with an intriguingly high theoretical capacity (approximately 10 times higher than that of conventional graphite anodes, that is 4200 mAh/g for the $Li_{4.4}Si$ accommodating more than 4 Li^+ per Si atom [2]). However, the severe volume change ($\sim$ 400%) associated with the repeated lithiation and delithiation processes hampers the mechanical/electrical integrity of Si anodes reducing the battery's life cycle [3–6] limiting the commercial exploitation of Si-based electrodes. Experimental investigations have revealed that silicon thin films [7,8], nanowires [9,10], and nanoparticles [11,12] exhibit considerably better performances in terms of capacity and cyclability than bulk Si.

A very promising approach to improve electrodes stability is to use functional polymer binders that play an important role in maintaining the structural, mechanical, and electrical integrity of the electrode [13–15]. These binders prevent pulverization of the active material, isolation, and agglomeration of active particles, and rupture of the solid electrolyte interface layer [16–20]. The required properties of a binder are manifold and identifying a proper one for different active materials is essential.

Polyvinylidene fluoride is the most commonly used polymer binder that works well in graphite anodes but fails in Si anodes

* Corresponding author.
E-mail address: rita.maji@unimore.it (R. Maji).

https://doi.org/10.1016/j.mtchem.2023.101474

because of poor adhesion to Si surfaces [21,22]. Many types of polymeric binders, either natural or synthetic, have been proposed to address the different challenges of active materials. Among those proposed for Si-based anodes, to name a few, there are poly[acrylic acid], polyamide imide, poly[vinyl alcohol] (PVA), polyethylenimine, polyacrylonitrile, polypyrrole, and so on [22]. In general, functional binders with −COOH and/or −OH groups maintain the interaction between binder and Si and are proposed for the long cycle stability of the Si electrodes [22,23].

Apart from the stability issues, also the electrochemical reactions with the electrolytes and the conducting properties have to be taken into account for a proper choice of binders. These last properties are obtained via the inclusion of conductive elements as carbon black and are modeled via inclusion of conjugated framework and free charge carries (donor/acceptor radicals), the most common are polyaniline (PANI), poly(3,4-ethylenedioxythiophene) (PEDT, PEDOT), polythiophene (PTh) [15,22].

In this paper, we address recently proposed self-healing polymers [24]. In particular, we focus on molecules (B-OH_PANI) where boronic acid ($-BO_2H_2$) groups are bonded to aniline units in the polymer backbone since this functional group is suggested as a potential candidate for tunable inter/intra molecular interaction [25,26]. PVA is also considered as a counter polymer, both by itself and in combination with B−OH_PANI. Hydrogen bond formation is assumed to take place between the free hydroxyl units of the boronic acid and the PVA. This bond formation is supposed to favor the healing of the electrode materials after decomposition or crack formation. Therefore, we are interested in exploring the adhesion properties of these systems to Si anode surfaces.

Adhesion to the active material surface is one of the most relevant issues in the choice of a binder. The adhesion strength is related to the synergic effect of the surface morphology and the binding properties of the polymeric binders. First-principles calculations can provide insight into processes at the atomic and electronic scales, still inaccessible to the experiment. The rationalization and design of the optimal polymer/active material interface geometry play a major role. The interface structure is influenced by several factors and a detailed characterization [27] of which is necessary: moreover, an atomistic knowledge of the binding mechanisms can help to tailor and optimize the properties of the Si/binder interfaces.

In this article, we discuss the binding mechanisms of B−OH_PANI and PVA monomers on differently oriented Si surfaces. The calculation details and the binder structures are described in Section 2. The results obtained for the structurally optimized binding geometries and consequent monomer/surface modifications are discussed in Sections 3.1 and 3.2. In Section 3.3, we further analyze the corresponding electronic configurations and charge transfers relevant in the binding mechanisms to the Si-surfaces. Very importantly, we shed some light on the role of the different surface orientations and of the monomer hydroxyl groups on the binding properties.

2. Method

To investigate the adhesion properties of different polymeric binders to Si-based anodes, we modeled the surfaces using Si slabs. Two different surface terminations, Si (110) and Si (111), were considered. We have chosen for the two orientations clean and unreconstructed surfaces that have dangling bonds differently oriented. We did not use the (7×7) reconstruction because it is too large and would have given problems in the lateral location of the monomers on the surface, since the sites are not equivalent. The final cell dimension of Si (110) and Si (111) is 15.36 Å × 16.29 Å × 28.68 Å and 15.36 Å × 19.95 Å × 29.01 Å, respectively. The binder unit adsorption is examined on one side of the slab, whereas the other side (bottom layer) is fully passivated using H atoms. We analyze the adsorption properties on the Si surfaces of two different monomers, namely boronic acid-doped polyaniline (B−OH_PANI) and PVA, shown in Fig. 1.

First-principles calculations were performed using a plane wave based implementation of DFT within Quantum Espresso [28], where the screened ionic potentials are approximated by *norm conserving* pseudopotentials [29]. The exchange-correlation contribution to total energy is estimated using a gradient corrected Perdew−Burke−Ernzerhof [30] functional. Minimum energy configurations of the monomers were obtained in the super cell using the BFGS [31] scheme of minimization of total energies. The plane wave cutoff on the basis set is 800 eV, and the $3 \times 3 \times 1$ k-mesh. The geometry optimization was iterated until the forces were less than $10^{-}3$ Rydberg/Bohr for all atoms. During the structural optimization, the bottom layers of the slabs are kept fixed.

For the calculation of the density of states of the optimized geometries, we used a $7 \times 7 \times 1$ k-mesh. For all configurations, the Van der Waals interaction was included through the vdW-DFT module [32].

To explore the interaction of the binders with the silicon surfaces, we considered a representative variety of initial configurations of the monomers, whose axes are differently oriented on the surfaces, as shown by red arrows in Figs. 2(a) and 3(a). This procedure leads to different groups/branches of the binder (−NH/$-BO_2H_2$/−OH) facing the surface plane in the initial configurations. The obtained optimized structures in their lowest energy configurations are investigated below. In the case of two monomers, we started from the lowest energy structure of one monomer on the surface and next consider different possible orientations for the second monomer. An alternative would be to consider both monomers in the initial configuration and optimize the ensemble but this strategy requires a much larger computational time to reach the ground state. A few tests performed to check the validity of our assumption in the case of a few configurations showed energy lowering within the range of ~0.02 eV and no relevant difference in the physical interpretation. The optimized structures of the slab together with the lowest energy configurations of one and two monomers of PVA and B−OH_PANI are presented in Figs. 2 and 3 for Si (110) and Si (111), respectively. The cases of one and two adsorbed monomers are referred to as low and high coverages, respectively.

3. Results and discussions

3.1. B−OH_PANI and PVA adsorption

The adsorption energy (E_A) of the monomers is calculated as

$$E_A = E_{slab+X} - E_{slab} - n_X E_X. \quad (1)$$

X are the adsorbed monomers, PVA and B−OH_PANI in our case. $E_{slab\ +\ X}$ and E_{slab} are the total energies of the optimized Si-slabs along with the monomers (PVA or/and B−OH_PANI) and of the Si slab (110/111), respectively. E_X is the total energy of the isolated binder unit calculated within the same supercell, and n_X is the number of monomers. In the case of cobinding [Fig. 2(f)], the energies of both the isolated monomers are considered in the equation. The calculated adsorption energies for all configurations with different monomers on the Si slab are given in Table 1.

3.1.1. Si(110) surface

The optimized Si (110) surface shows an atomic buckling involving the first two layers of the slab [Fig. 2(a)]. The optimized

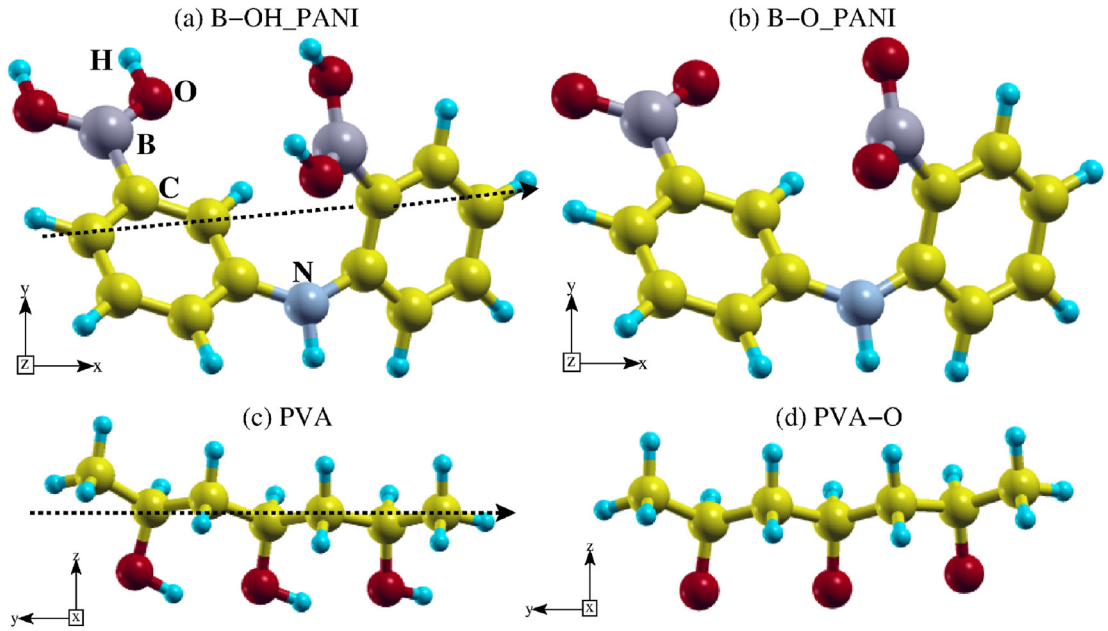

Fig. 1. Molecular structure of the monomers used in this study: (a) B–OH_PANI, (b) B–O_PANI (H removed from $-BO_2H_2$ group), (c) PVA, (d) PVA-O (H removed from –OH group). The dotted arrow represents the molecular axis. B–OH_PANI, boronic acid-doped polyaniline; PVA, polyvinyl alcohol.

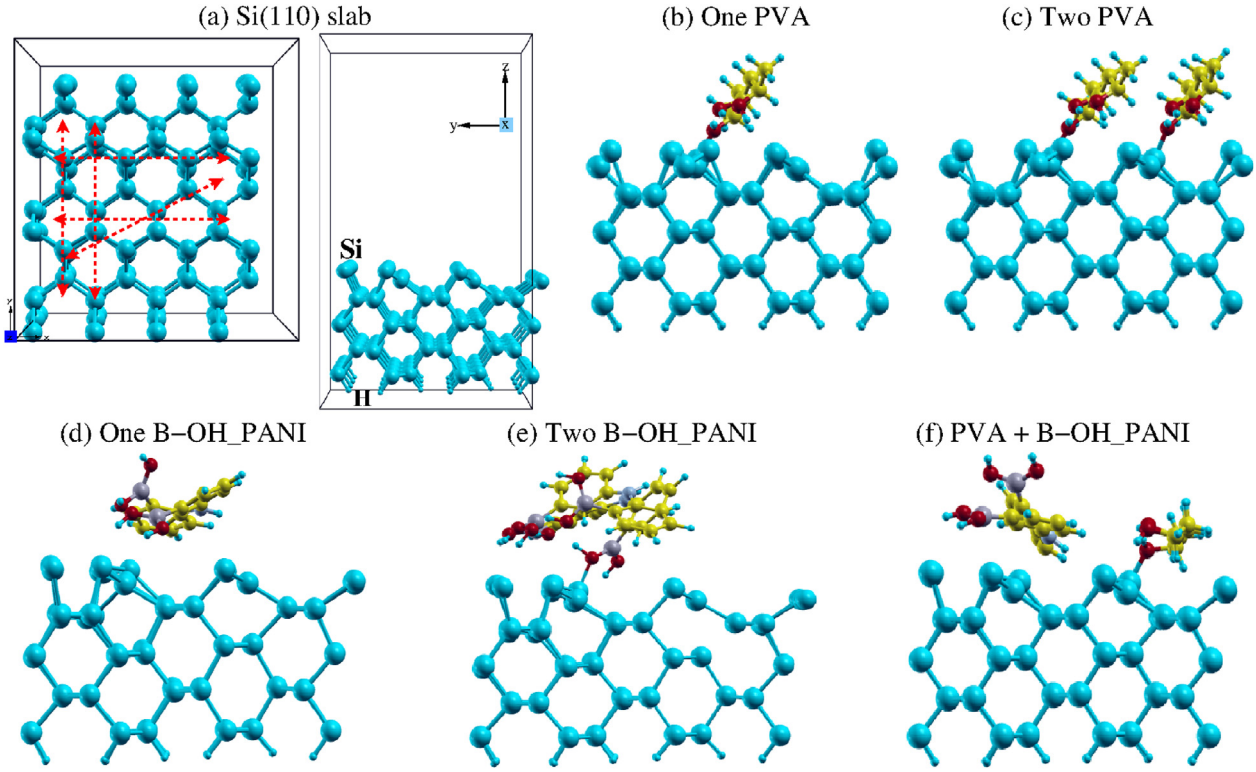

Fig. 2. Si (110) slab (a) optimized surface with x-y, y-z planar view, and along with binders: (b) one PVA, (c) two PVA, (d) one B–OH_PANI, (e) two B–OH_PANI, (f) one PVA and B–OH_PANI together. For all the systems, final optimized structures are presented. Red arrows in (a) schematically represent different initial positions of the binder.

configuration with one PVA monomer shows a more pronounced distortion of the same surface Si layers. Fig. 2(b) shows that one of the oxygens of PVA forms a Si–O bond 1.823 Å long with the nearest unsaturated Si atom. This bond is much more elongated compared to the Si–O bond in bulk SiO_2 (1.62 Å). This weak bond leads to a small elongation of the nearby O–H and C–O bonds in the linear PVA chain. In the presence of a second PVA monomer, the Si surface remains almost unchanged without additional distortion and we can see in Fig. 2(c) that the two monomers attach to the surface apart from each other. Also, the second PVA is anchored to the surface through the O atom forming a similar elongated Si–O bond (1.83 Å). As a consequence, the adsorption energy E_A of the

Table 1
Adsorption energy (eV) of PVA and B−OH_PANI on the Si (110) and Si (111) slabs. The values are reported only for the lowest energy structures.

X	Si(110) (eV)	Si(111) (eV)
One PVA	−1.587	−5.073
Two PVA	−3.160	−6.429
One B−OH_PANI	−1.554	−5.849
Two B−OH_PANI	−2.468	−7.241
One PVA + One B−OH_PANI	−3.478	−7.523

configuration with two monomers is about twice the E_A of one monomer [Table 1], which confirms that the intermolecular interaction between the two monomers is very weak.

The adsorption of one and two B−OH_PANI (Fig. 2(d, e)) monomers does not distort the Si-surface significantly, in contrast to the PVA case. Moreover, the B−OH_PANI tends to orient itself facing the −OH (group from -BO_2H_2) to the surface but without forming any bond. In the adsorption of two B−OH_PANI monomers, a Si−O bond is formed (1.86 Å), the molecules tend to be parallel to each other and the -BO_2H_2 groups try to rotate in order to reduce the steric repulsion.

In the coadsorption of one PVA and one B−OH_PANI (Fig. 2(f)), the surface distortion created by the previous adsorption of the PVA monomer helps to stabilize the additional B−OH_PANI monomer oriented parallel to the surface. We infer this result by observing that the distance (~2.18 Å) of B−OH_PANI from the Si-surface is now shorter than the distance from the surface of the same monomers without coadsorption with PVA. The intermolecular interaction between PVA and B−OH_PANI also causes the adsorption energy to be lower than the sum of the adsorption energies of the two single monomers (Table 1). Thus, our results show that the coabsorption of B−OH_-PANI with PVA is going to improve the adhesion properties of the polymers to the (110) Si-surface.

3.1.2. Si(111) surface

In Fig. 3, the optimized Si (111) slab and lowest energy adsorption configurations of one or two monomer(s) of PVA and/or B−OH_PANI are presented. The adsorption of one PVA monomer is associated with a strong reconstruction, which is evident in the first two Si layers (Fig. 3(b)). Two of the O atoms saturate the Si sites forming weak Si−O bonds with bond lengths 1.91 Å and 1.93 Å, which thus elongate the C−O bonds, as already discussed for Si (110). This all together leads to strong adsorption energy. When two PVA (Fig. 3(c)) are adsorbed, three Si−O bonds (1.91 Å) are observed, together with an increased distortion of the surface, which explains the small reduction of adsorption energy (see Table 1).

The reconstruction of the Si surface and the bending of the monomer towards the surface is clearly a sign of strong physisorption of B−OH_PANI, (Fig. 3(d)). When a second B−OH_PANI monomer is added, the intermolecular interaction induces a rotation of the second monomer so as to involve a larger number of unsaturated Si sites. The Si surface does not suffer any additional corrugation, and the adsorption energy lowers considerably as a consequence of the larger exposition of the monomers to the surface. The lower gain in adsorption energy [Table 1] associated with the two B−OH_PANI could be related to the fact that the configuration of the second monomer is strongly distorted and its orientation is not energetically favorable as for the one facing the -BO_2H_2 group to the surface. As in the case of the Si (110) surface, the second monomer rotates in such a way that the −OH from -BO_2H_2 group are closer to each other at a distance O−H = 1.81 Å.

Finally, we analyze the case of coadsorption of PVA and B−OH-_PANI on the Si (111) slab. The two monomers arrange themselves by establishing hydrogen bond based interactions, both between them and with the substrate, that involve the −OH group of PVA and -BO_2H_2 group of B−OH-_PANI. Moreover, the coadsorption arrangement is driven by the maximization of the surface coverage (Figs. 2(f), 3(f)). We find that the adsorption energy is enhanced by the coadsorption of the two monomers, alike for the Si (110) surface. In addition, the coadsorption of PVA and B−OH_PANI increases the adhesion of both monomers: the cobinder functionalized surface is more stable with respect to the case when the two binder units are of the same kind (two PVA/two B−OH_PANI). Thus, the coabsorption of B−OH_PANI and PVA will be beneficial for the binder adhesion properties for both the Si facets.

From the adsorption energy values (Table 1), it is evident that the adhesion of these polymeric monomers is larger for (111) than for (110), due to Si passivation/saturation effects. It is likely that a contribution to the larger adsorption energy for (111) orientation could be due to the excess of dangling bonds on our ideal surface relative to the stable reconstructed 7 × 7 surface.

In the case of the (110) surface, the double functionalization does not entail a large intermolecular interaction, since the two monomers behave almost independently (as confirmed also by absorption energies shown in Table 1). For both substrates, we notice that two PVA tend to stay farther apart than two B−OH_PANI. Still, we must notice that cobinding is preferred with respect to cases where the binders are of the same type. Conversely, the adsorption of a second monomer on the (111) substrate implies a strong coupling with the first one that hinders the interaction with the substrate (geometry is also deformed), and this is reflected by the small energy increase gained by the addition of the second binder. However, we can still notice that double functionalization with different monomers is preferred.

Even if most of the analyzed configurations are either physisorbed or weakly bonded to a few Si atoms, we remark that surface reconstruction plays a major role in lowering the adsorption energy.

3.2. B−O_PANI and PVA-O adsorption

From the previous analysis, we have seen that the presence of the hydroxyl group in PVA and B−OH_PANI favors the attraction of the molecules to the surfaces and their mutual interaction. Since the oxygen atoms are fully coordinated, these interactions are mainly electrostatic, even if some weak bonds can form with the unsaturated surface Si atoms. Thus, it can be interesting to compare the weak adsorption of the fully hydrogenated binders analyzed above with the full Si-surface functionalization with similar molecular groups without H. In this case, the molecules are strongly anchored to the surface through the removal of the H atoms from the hydroxyl groups, as shown in Fig. 1(b, d). The H removal opens the oxygen coordination allowing for the formation of much stronger Si−O bonds with the Si atoms of the surface.

Also for this case, we have explored different configurations of which only the most interesting features are described in detail below. In the following, we assume the removed hydrogen atoms end up in a reservoir of hydrogen gas. The energetics of this process is calculated as:

$$E'_{\mathrm{A}} = E_{\mathrm{final}} + n_H E_{\mathrm{H}} - E_{\mathrm{slab}} - n_{\mathrm{X}} E_{\mathrm{X}}. \quad (2)$$

E_{final} is the total energy of the final optimized structure, that is, surface with the adsorbed molecule(s), n_H is the number of H atoms removed from the monomers, E_H is half the energy of an isolated H_2 molecule within the same simulation cell, E_{slab} and E_{X} are same as in Eq. (1).

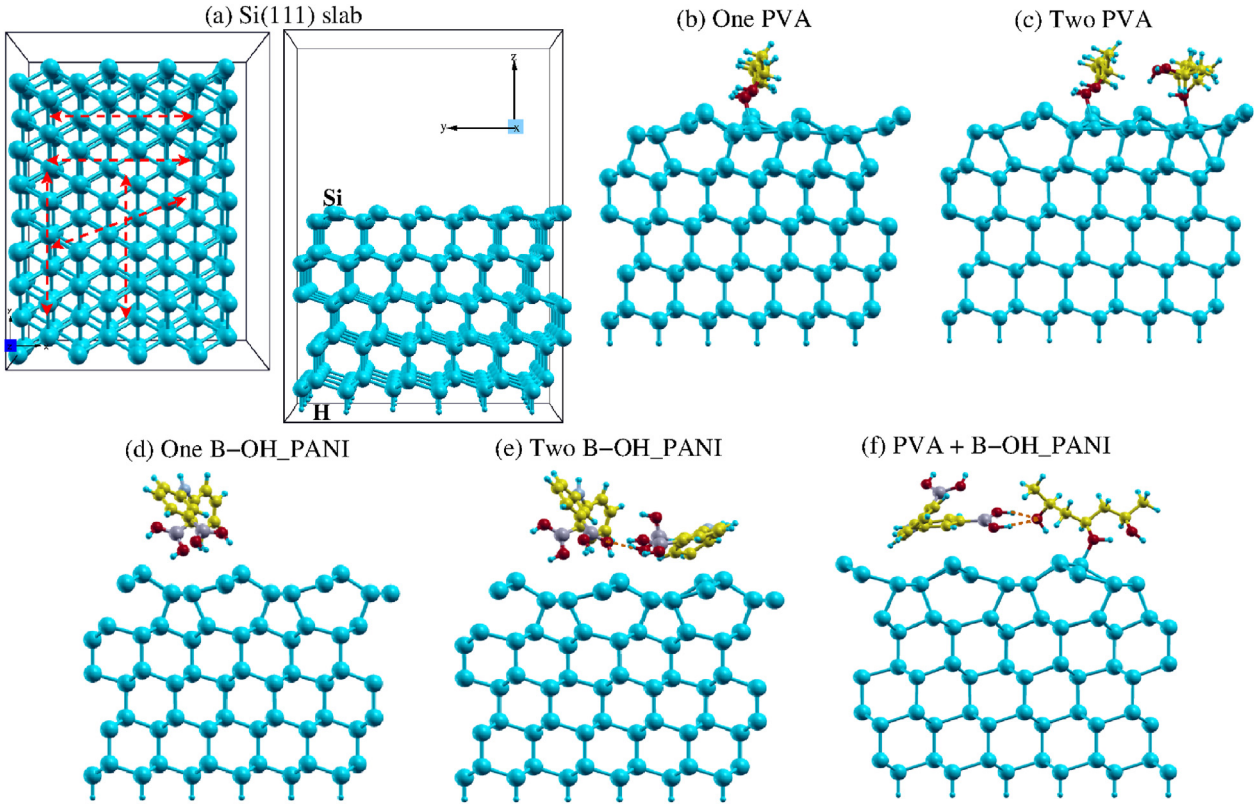

Fig. 3. Si (111) slab (a) optimized surface with x-y, y-z planer view, and along with binders: (b) one PVA, (c) two PVA, (d) one B–OH_PANI, (e) two B–OH_PANI, (f) one PVA and B–OH_PANI together. For all the systems, final optimized structures are presented. The red arrows in (a) represent different initial positions of the binder schematically.

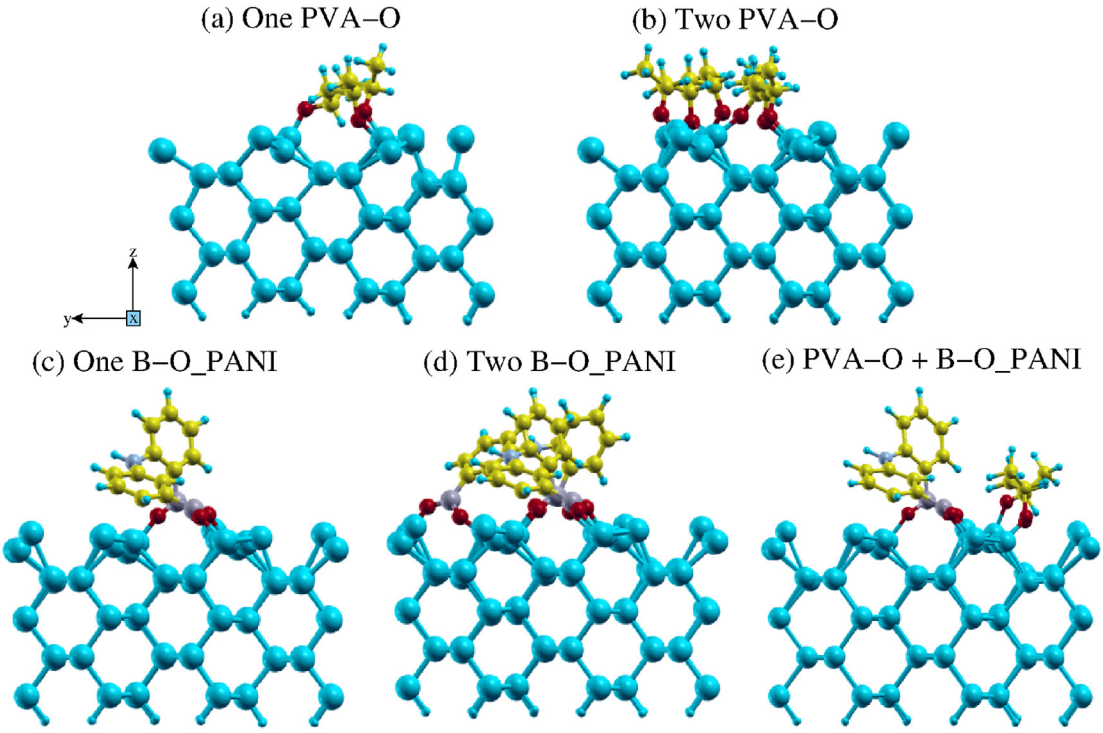

Fig. 4. Si (110) slab with (a) one PVA-O, (b) two PVA-O, (c) one B–O_PANI, (d) two B–O_PANI, (e) one PVA-O and B–O_PANI together. Here, monomers are according to Fig. 1(b, d). Optimized geometry for all the configurations is presented here. B–OH_PANI, boronic acid-doped polyaniline; PVA, polyvinyl alcohol.

We have calculated E'_A also using the energy of the hydrogen atoms passivating the silicon surface dangling bonds instead of the energy of the hydrogen atoms of the H_2 molecule to simulate the physical situation where the removed H attach to the surface. We obtained adsorption energies as low as −30 eV to −40 eV. This considerable lowering of the adsorption energies is due to the strong Si−H bonds and makes it more difficult to extract the contribution of the molecule(s) adsorption, which is the main objective of the paper. This is the reason we prefer to use gaseous hydrogen.

The PVA monomer without H at the −OH sites forms very strong bonds between all the available unsaturated O sites with the Si atoms on the Si (110) surface (Fig. 4(a)). The Si−O bond lengths (1.66−1.68)Å are similar to those of bulk SiO_2. The lowest energy structure with two PVAs (Fig. 4(b)) adsorbed on Si (110) shows a scenario, where at least one of the Si atom is shared between two O atoms of two monomers and the monomer prefers relatively close proximity than the previous case. Here, all Si−O bonds are within (~1.63−1.69)Å, and with one elongated bond (1.78 Å) shared with the O of the second monomer.

For B−O_PANI (Fig. 4(c)), all O atoms are bonded with Si and Si−O bond lengths are in the range of (1.66−1.71)Å. The monomer, even within this strong chemical bonding environment preserves the bending structure with respect to N ($\angle C{-}N - C = 128.735°$) compared to optimized structures of the monomer at vacuum state ($\angle C{-}N - C = 128.038°$). However, the presence of a second monomer [Fig. 4(d)] leads to a much distorted geometry of the binders ($\angle C{-}N - C = 131.781°$ and 118.402°) although it does not affect the Si−O bonding (bond length 1.66−1.71 Å). For coadsorption (PVA-O + B−O_PANI) (Fig. 4(e)), all O atoms are bonded to single Si sites (Si−O ~1.68−1.71 Å).

Table 2
Adsorption energy (eV) of PVA and B−O_PANI on Si (110) and Si (111) slab. The values are reported for the lowest energy structures. Initial configurations are considered without H at −OH (Fig. 1b, d) on the monomer.

X	Si(110) (eV)	Si(111) (eV)
One PVA-O	−3.963	−5.738
Two PVA-O	−5.514	−8.811
One B−O_PANI	−4.859	−5.768
Two B−O_PANI	−9.892	−9.978
PVA-O + B−O_PANI	−8.350	−9.737

For Si(111) surface, the presence of unsaturated oxygen atoms also favors strong chemical bonding. All oxygen atoms are in fact involved in covalent Si−O bonds: Si atoms bond with one (Fig. 5(a)) or two oxygen atoms (Fig. 5(a, b)). In the case of two PVA-O monomers, instead of parallel orientation, as it happens for two PVA on Si(111), they prefer a cross orientation to each other, even if the initial configuration corresponds to parallel orientation, which allows to maximize the number of Si−O bonds.

In the case of B−O_PANI with one and two monomers (Fig. 5(c, d)), we observed a strong distortion of the binder. In fact, one of the unsaturated O atoms bonds with the C of the other ring, as marked by the red arrow in x-y planar view of Fig. 5(d). All other O atoms bond with the Si sites (Si−O ~1.69 Å) like in all previous configurations. For coadsorption (Fig. 5(e)), all Si−O bonds are equivalent to the corresponding single monomer (PVA-O/B−O_PANI) structure of both of them. Reconstruction of the surface is relatively small in both cases.

From Tables 1 and 2, it is evident that without the formation of such a chemical bonding, the adsorption energy is always lower: the formation of Si−O bond is associated with an overall increase of

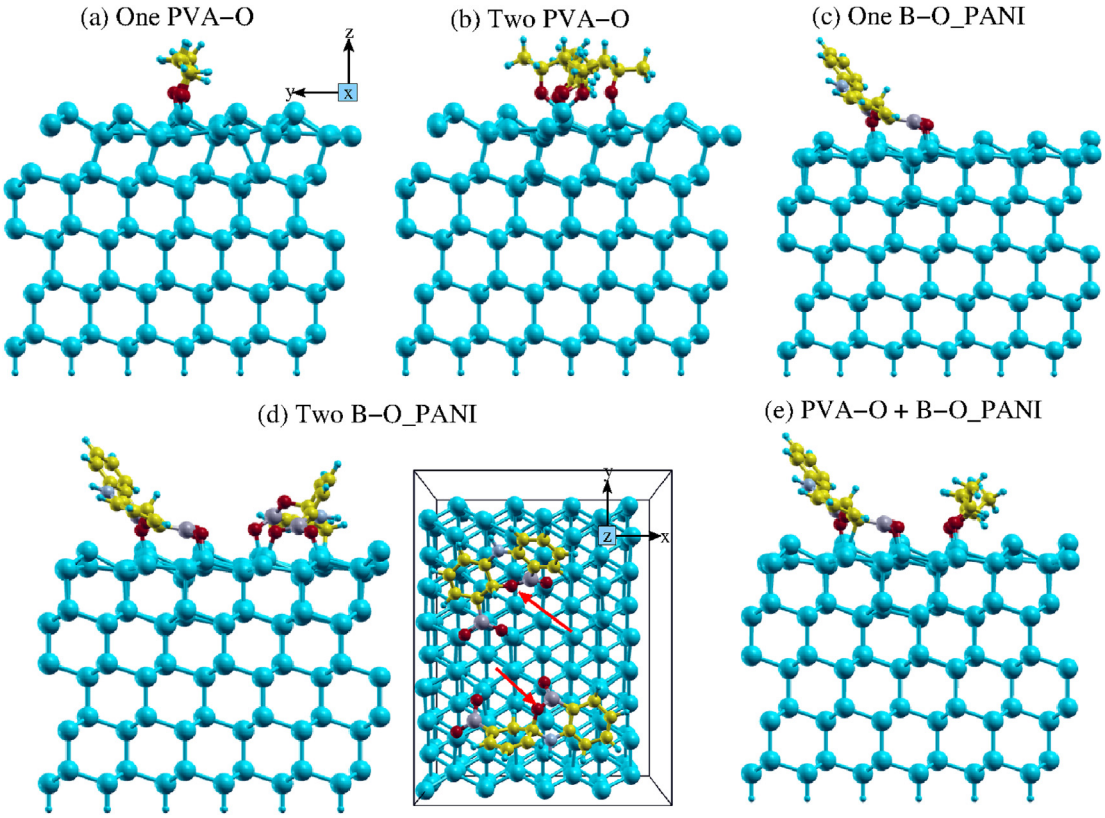

Fig. 5. Si (111) slab with (a) one PVA-O, (b) two PVA-O, (c) one B−O_PANI, (d) two B−O_PANI (y-z and x-y planar view), (e) one PVA-O and B−O_PANI together. Here, monomers are according to Fig. 1(b, d). Optimized geometry for all the configurations is presented here. B−OH_PANI, boronic acid-doped polyaniline; PVA, polyvinyl alcohol.

the adsorption energy (maximum enhancement is ~2.5 eV). Table 2 confirms the picture that we extracted from structural analysis: when two monomers are adsorbed, they behave quite independently from each other, especially in the case of Si(110).

3.3. Analysis of electronic properties

To better understand the obtained results, a detailed analysis of the electronic structure at the interfaces is necessary. We focus on the charge densities, the density of states (DOS), and the electron localization function (ELF) analysis. A few of the structures from Sections 3.1 and 3.2 are considered for further analysis.

A popular form of showing electronic structure of the interface is the charge distribution that clearly shows the chemical environment of the atoms, which is difficult to be measured by experiments. For this, the charge density difference is calculated as:

$$\Delta\rho = \rho(s+b) - \rho(s) - \rho(b) \quad (3)$$

where ρ(s + b), ρ(s), and ρ(b) correspond to the charge density of the slab with a binder, slab, and binder system, respectively.

For the binder with unsaturated O (PVA-O, B—O_PANI), to understand the evolution of the bonding structure under strong chemisorption, we have analyzed the behavior of ELF.

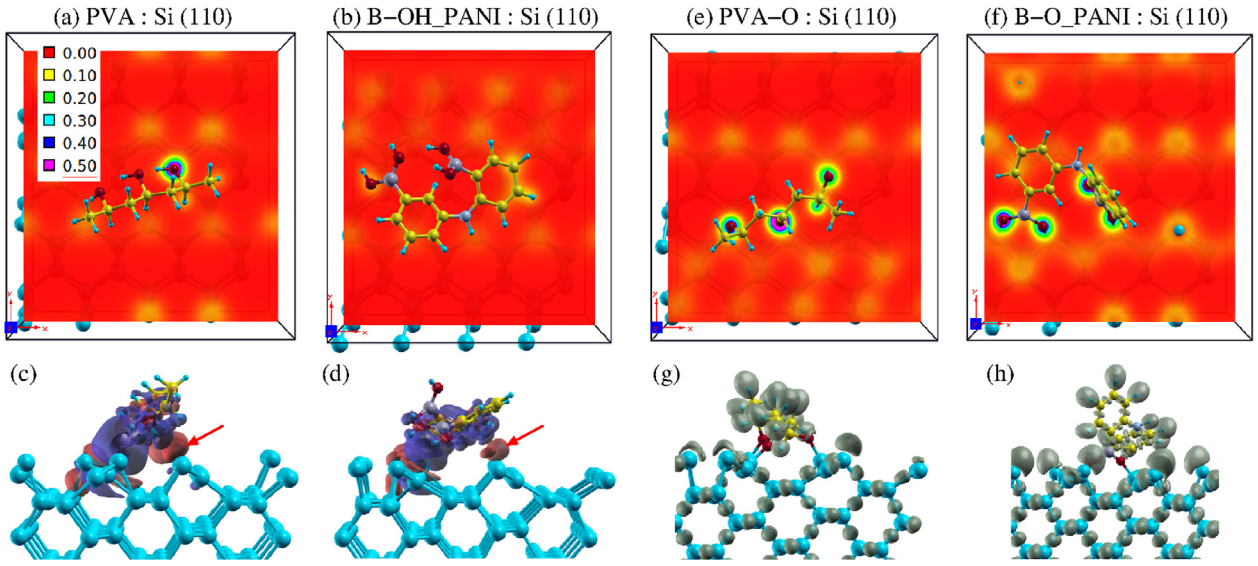

Fig. 6. Upper panel: projection of charge density at the interface of Si (110) slab with one (a) PVA, (b) B—OH_PANI, (e) PVA-O and (f) B—O_PANI. Contour values are listed in (a). Lower panel: charge density difference ($\Delta\rho$) (c) PVA, (d) B—OH_PANI with isovalue 0.001. In (c, d), red and blue color isosurface represent charge accumulation and depletion, respectively. ELF plot of (g) PVA-O and (h) B—O_PANI.

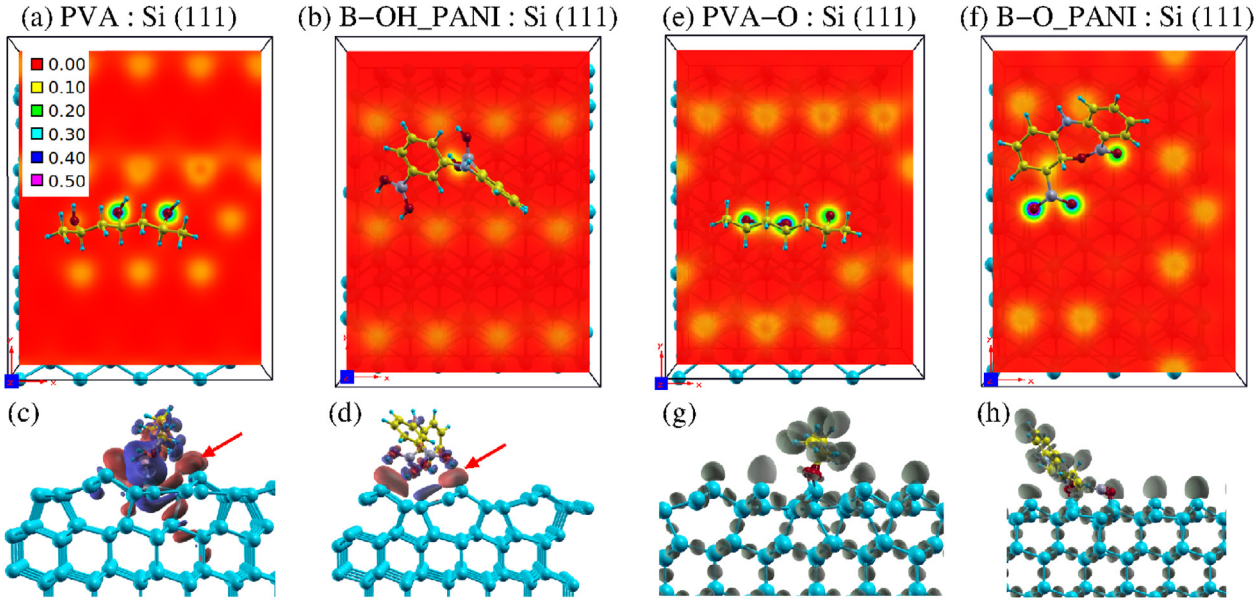

Fig. 7. Upper panel: projection of charge density at the interface of Si (111) slab with one (a) PVA, (b) B—OH_PANI, (e) PVA-O, and (f) B—O_PANI. Contour values are listed in (a). Lower panel: charge density difference ($\Delta\rho$) (c) PVA, (d) B—OH_PANI with isovalue 0.001. In (c, d), red and blue color isosurface represent charge accumulation and depletion, respectively. ELF plot of (g) PVA-O and (h) B—O_PANI.

The charge density distributions shown in Fig. 6(a, b, e, f) allow us to identify the atoms which contribute significantly to interfacial bonding and strong contributions are recognizable by high charge densities in the plane between the Si slab and the attached binder. With PVA (Fig. 6(a)), only a weak density is observed around O bonded to Si; however, for B–OH_PANI, no such region exists around O. Instead around two of the C sites (Fig. 6(b)), a relatively weak contour density is observed. In order to quantify the charge transfer related to the interface bonding, we analyzed the charge density difference $\Delta\rho$ as shown in Fig. 6(c, d). Apart from the larger charge depletion (blue isosurface) at Si sites bonded to O, it shows the accumulation (red isosurface) at other parts of the surface as marked by the red arrow in Fig. 6(c, d). These are the surface Si sites where some parts of the monomer are nearby (~ 2.7 Å). The charge transfer is due to the weak interaction between those Si sites relatively closer to the hydrogen of the rotated CH bonds (for PVA)

Table 3
The Löwdin charge of binder and adjacent/bonded Si site with single PVA, B–OH_PANI, PVA-O, and B–O_PANI at Si (110) and Si (111) slab. The values are reported for the selected sites adjacent to the binder for the physisorbed scenario and bonded Si site in all other cases. Values for the final system (slab + binder) are compared with that for Si slab(s) and isolated binder(s).

Binder	Atom	Charge(*e*): Si(110)	Charge(*e*): Si(111)	Note
PVA	Si	3.79/3.57	3.99/3.59	slab(s)/slab + binder(s + b)
	O	6.54/6.46	6.54/6.42	b/s + b
PVA-O	Si	3.79/3.39	3.99/3.37	s/s + b
	O	6.54/6.55	6.54/6.55	b/s + b
B–OH_PANI	Si	3.79/3.99	3.99/4.13	s/s + b
	O	6.54/6.49	6.54/6.51	b/s + b
B–O_PANI	Si	4.09/3.44	3.99/3.39	s/s + b
	O	6.53/6.57	6.53/6.57	b/s + b
	B	2.45/2.49	2.45/2.46	b/s + b
	N	5.28/5.22	5.28/5.22	b/s + b

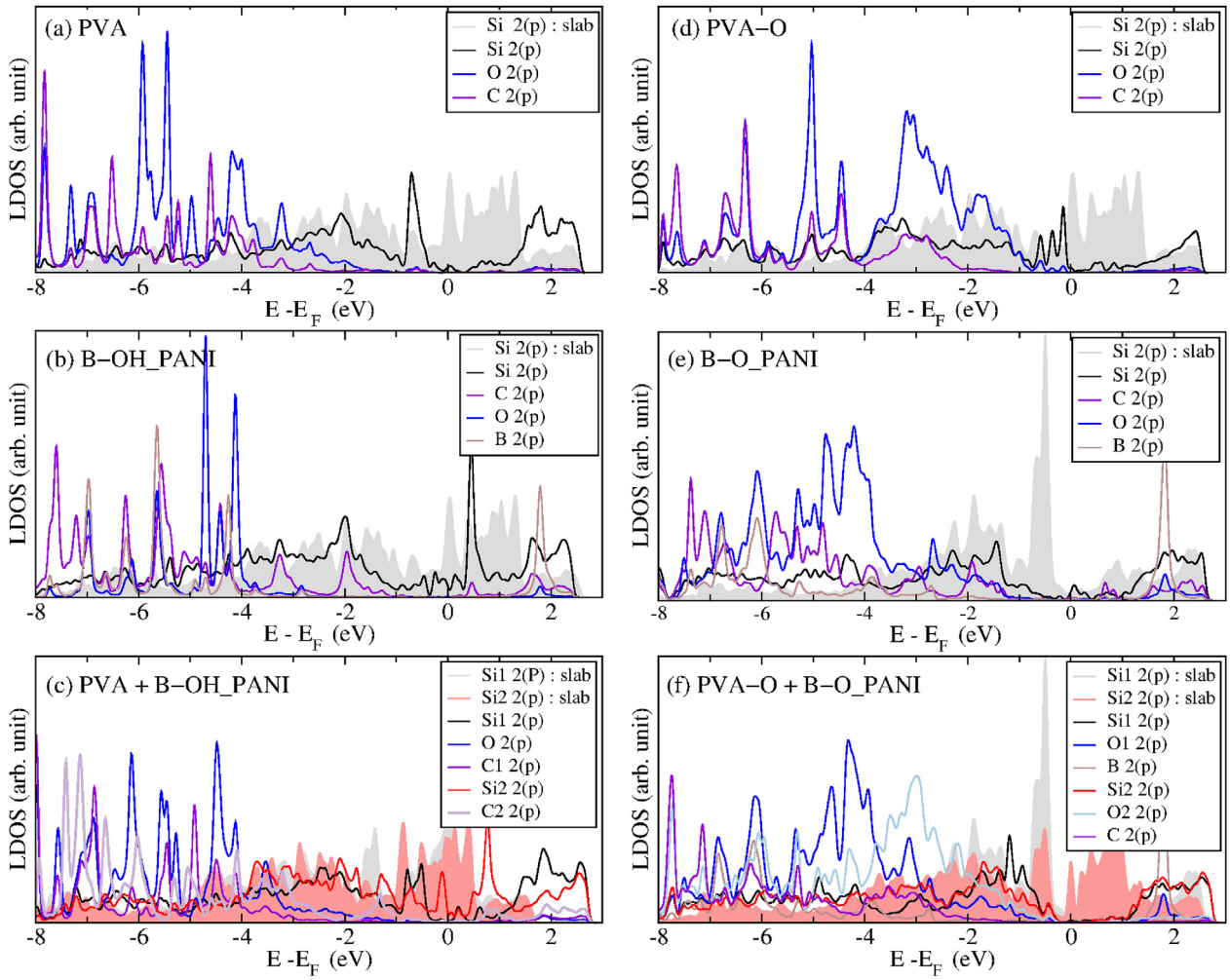

Fig. 8. Projected density of states of Si (110) surface with one (a) PVA, (b) B–OH_PANI, (c) PVA and B–OH_PANI together and (d) PVA-O, (e) B–O_PANI, (f) PVA-O and B–O_PANI together. For all structures, the same Si sites in the absence (slab) and presence of the binder are plotted for comparison. We considered only the LDOS of O, C, and B sites bonded to Si or in close proximity to the Si surface. B–OH_PANI, boronic acid-doped polyaniline; PVA, polyvinyl alcohol.

or to the C ring (for B–OH_PANI). Therefore, the physisorbed configurations adopted by these binders—even without the formation of chemical bonding—show strong electronic charge transfer at the interface, in agreement with large adsorption energy values.

Now, for the monomer without H (i.e. PVA-O and B–O_PANI), charge density distribution at the interface is shown in Fig. 6(e, f), respectively. The strong Si–O binding for these systems is clearly evident from the enhanced value of the density contour. 3D ELF isosurface shows strong localization at the surface Si sites, while for Si within tetrahedral coordination from following layers, ELF is localized at Si–Si covalent bonded sites (Fig. 6(g, h)). Deformation of the ELF isosurface represents the bond strain. Small localization is also visible around O sites bonded to Si.For Si (111) (Fig. 7), similar charge density analysis is performed. Fig. 7(a) shows two high-density contours along the Si–O bonds with PVA, and it shows relatively lower charge densities with B–OH_PANI (Fig. 7(b)). This is also evident from Fig. 7(c, d), where charge accumulation and depletion is more prominent for PVA, while with B–OH_PANI only accumulation at distorted Si surface occurs. However, both binders show a quite strong impact on interfacial morphology even with small charge transfer processes. Charge density distributions for the structures with PVA-O (Fig. 7(e)) and B–O_PANI (Fig. 7(f)) clearly demonstrate a significantly increased covalent contribution in the interfacial bonding. In addition, delocalization of ELF across the Si bonds confirms the distortion of the first two Si layers with PVA-O (Fig. 7(g)) that is instead less affected in presence of B–O_PANI (Fig. 7(h)).

More quantitative understanding is possible from values of Löwdin charges, for selected sites adjacent to a binder for physisorbed scenario and bonded Si site in all other cases, as summarized in Table 3. Löwdin analysis confirms that the Si, bonded to O in PVA, shows a charge depletion for both Si (110) and Si (111) surfaces, and this is more enhanced with PVA-O, as expected considering the already cited strong chemical bonding. Notably, B–OH_PANI on Si (110) shows an enhanced charge transfer between Si and C (Si–C = 2.15 Å), with accumulation around C (4.14*e* before and 4.25*e* afterward) and depletion from Si (3.79*e* before and 3.71*e* afterward) as already observed in (Fig. 6(d)).

However, with B–O_PANI, B has two different types of coordination: in one case, where the B atom is attached to two O atoms that finally bonded to Si, there is a weak charge transfer as shown in Table 3, whereas when the B atom has one bond with O which is then connected to C (the O atom marked with red arrows in Fig. 5(d)), a strong depletion is found (6.53*e*/6.34*e*): this rearrangement of the electronic charge within the molecule is strictly connected to its strong distortion upon adsorption.

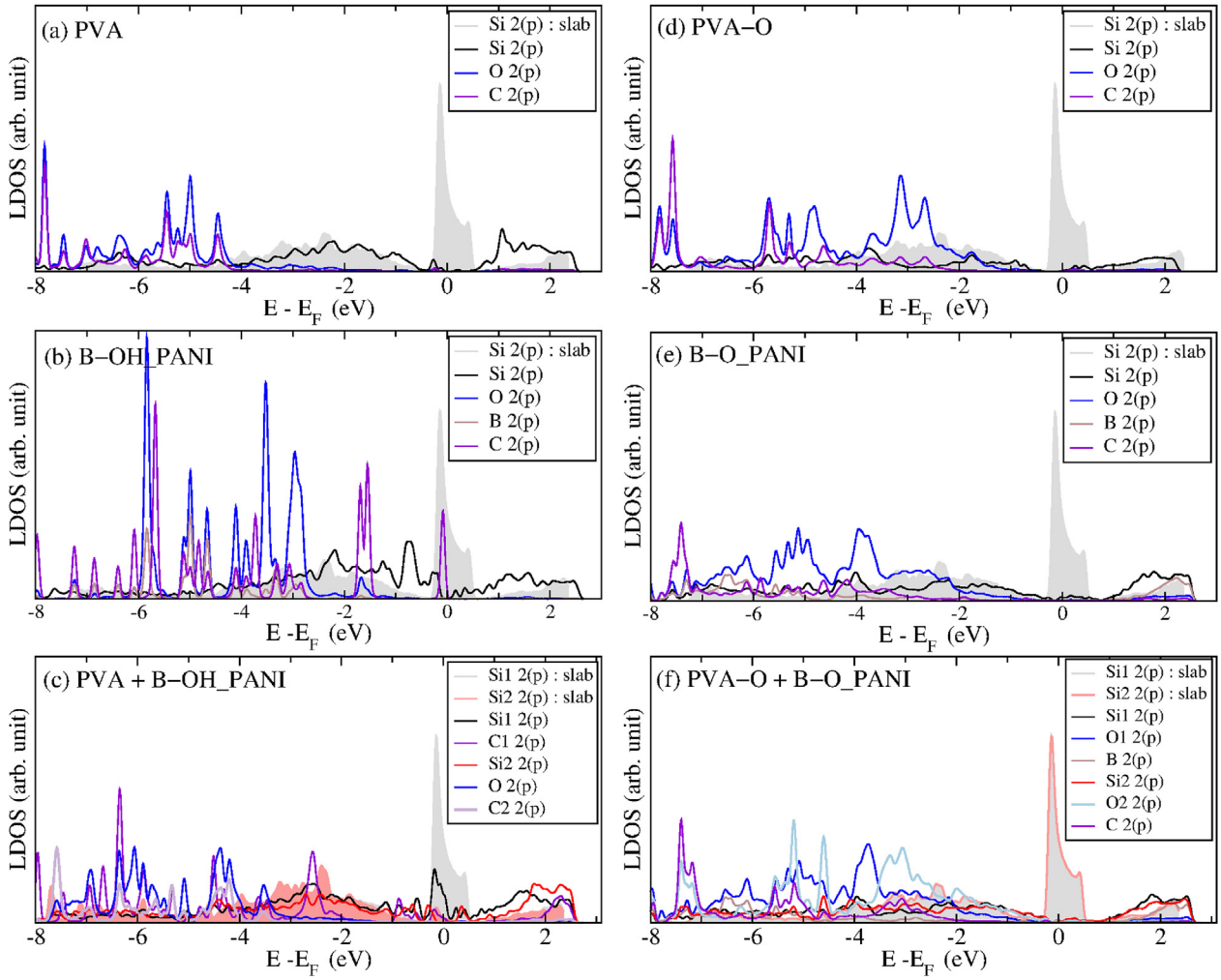

Fig. 9. Projected density of states of Si (111) surface with one (a) PVA, (b) B–OH_PANI, (c) PVA and B–OH_PANI together and (d) PVA-O, (e) B–O_PANI, (f) PVA-O and B–O_PANI together. For all structures, the same Si sites in the absence (slab) and presence of the binder are plotted for comparison. We considered only the LDOS of O, C, and B sites bonded to Si or in close proximity to the Si surface. B–OH_PANI, boronic acid-doped polyaniline; PVA, polyvinyl alcohol.

Figs. 8 and 9 show the local density of states (LDOS) obtained from sum of projection of atomic orbitals. Here, LDOS of the Si sites in close proximity/bonded to binders and those (O/C/B) of the binders are plotted. As a result of adsorption on Si (110) (Fig. 8(a–f)), the p bands around the Fermi energy of fully/partially saturated Si are almost suppressed. The suppression of unsaturated Si 2(p) states is stronger in the case of PVA-O, B–O_PANI, and PVA-O + B–O_PANI (Fig. 8(d–f)), as expected. In general, the molecule absorption does not impact so much on the other orbitals (C and B atoms), since the corresponding states are far below with respect to the Fermi energy (Fig. 8(a–f)), despite of the close proximity even for strongly bonded configurations, with the only exception of C-derived states of B–OH_PANI (Fig. 8(b)). We also notice that, in the cases where strong Si–O bonds are formed, the oxygen-projected states are closer to the Fermi energy and the overall overlap with the Si states is much larger (Fig. 8(d–f)). Similar findings apply to Si (111) case (Fig. 9), with the only exception for C, states in B–OH_PANI and B–O_PANI (Fig. 9(b, e)) where the C peak at the Fermi energy disappears once the B–O–C configuration, as marked in Fig. 5(d), takes place with B–O_PANI.

4. Conclusion

In the present work, we systematically investigated, through *ab-initio* calculations, the structural and electronic properties of the interfaces between different Si-surfaces (Si (110) and Si (111)) and two specific binders (PVA and/or B–OH_PANI). The analysis of configurations involving one/two PVA monomers indicates good adhesion properties, with adsorption energy larger for (111) than for (110) Si surface. Here, the major role in the adsorption mechanism is played from one side by the formation of elongated Si–O bonds between the monomers and the surface Si atoms, and from the other side by the surface distortion of the relaxed systems after the anchoring of the binders. In the case of one/two boronic acid-doped polyaniline monomers, although the binders undergo only physisorption, the $-BO_2H_2$ functional group reveals strong adhesion properties. Also, in this case, we found a different behavior for the two considered surfaces. In fact, the distorted molecular structures with -BO_2H_2 towards the Si surface together with the intermolecular interactions impacted much of the interface structure in the case of Si (111). Conversely, the parallel orientation of B–OH_PANI on the Si(110) surface, while energetically preferable, prevents the absorption of a second monomer thereby reducing the overall adhesion in a high-coverage regime.

The investigation of co-binder configurations reveals a strong intermolecular interaction between PVA and B–OH_PANI on both the Si surfaces: this indicates that the co-polymer configuration maximizes the adhesion properties on both surfaces, with a larger gain in adsorption energy for the Si (111) surface.

The hydroxyl groups of the two monomers seem to be one of the main factors that drive both the interaction between them and with the surface. The modification of the surface layers and the bonding mechanism between surface and monomers impact the electronic properties of the active material and therefore on the performance of LIBs: our results highlight the fact that multiple mechanisms are playing a role at the Si-binders interface. A promising perspective opened by our study concerns the investigation of self-healing effects related to the cross-linking configurations of these polymers on Si-surfaces by means of a realistic bulk binder model.

Credit author statement

Rita Maji: performing calculation, methodology, formal analysis, writing original draft.

Michele A. Salvador: methodology, analysis, and discussion of the results.

Alice Ruini: supervision, formal analysis, writing – review and editing, funding acquisition.

Rita Magri: supervision, formal analysis, writing – review and editing, funding acquisition.

Elena Degoli: supervision, formal analysis, writing – review and editing, funding acquisition.

Declaration of competing interest

The authors declare that they have no known competing financial interests or personal relationships that could have appeared to influence the work reported in this paper.

Data availability

The data that has been used is confidential.

Acknowledgment

This research was developed under the framework of the BAT4-EVER project that has received funding from the European Union's Horizon 2020 research and innovation program under Grant Agreement No 957225. R. Maji would like to thank the University of Modena and Reggio Emilia for the financial support (FAR2020 and FAR2021). The authors would also like to acknowledge the CINECA HPC facility for the approved ISCRA B (IsB25_POLYFACE) and ISCRA C projects (IsC90_Interpol, IsC96_SEE-NOW). A.R.,E.D., and R.M. acknowledge the *PNRR MUR project ECS_00000033_ECOSISTER*. E.D. and R.M. acknowledge the MOST e Sustainable Mobility Center funded by the European Union Next-GenerationEU (PIANO NAZIONALE DI RIPRESA E RESILIENZA (PNRR) e MISSIONE 4 COMPONENTE 2, INVESTIMENTO 1.4 e D.D. 1033 June 17, 2022, CN00000023). This manuscript reflects only the authors' views and opinions, neither the European Union nor the European Commission can be considered responsible for them.

References

[1] D. Chen, D. Wang, Y. Yang, Q. Huang, S. Zhu, Z. Zheng, Self-healing materials for next-generation energy harvesting and storage devices, Adv. Energy Mater. 7 (23) (2017), 1700890.
[2] C.K. Chan, H. Peng, G. Liu, K. Mcilwrath, X. Fengzhang, R.A. Huggins, Y. Cui, High-performance lithium battery anodes using silicon nanowires, Nat. Nanotechnol. 3 (2008) 31–35.
[3] S.J. Lee, J.K. Lee, S.H. Chung, H.Y. Lee, S.M. Lee, H.K. Baik, Stress effect on cycle properties of the silicon thin-film anode, J. Power Sources 97–98 (2001) 191–193.
[4] L.Y. Beaulieua, T.D. Hatcharda, A. Bonakdarpoura, M.D. Fleischauera, J.R. Dahna, Reaction of Li with alloy thin films studied by in situ AFM, Electrochem. Soc. 150 (2003) A1457.
[5] Wei Wang, Prashant N. Kumta, Reversible high capacity nanocomposite anodes of Si/C/SWNTs for rechargeable Li-ion batteries, J. Power Sources 2 (172) (2007) 650–658.
[6] C. Wang, H. Wu, Z. Chen, M.T. McDowell, Y. Cui, Z. Bao, Self-healing chemistry enables the stable operation of silicon microparticle anodes for high-energy lithium-ion batteries, Nat. Chem. 5 (2013) 1042.
[7] J.P. Maranchia, A.F. Heppb, A.G. Evansc, N.T. Nuhfera, P.N. Kumta, Interfacial properties of the a-Si/Cu :Active-Inactive thin-film anode system for lithium-ion batteries, Electrochem. Soc. 153 (6) (2006) A1246.
[8] Haodong Li, Haoyu Li, Yizhu Lai, Zhiwei Yang, Qing Yang, Yang Liu, Zhuo Zheng, Yuxia Liu, Yan Sun, Benhe Zhong, Zhenguo Wu, Xiaodong Guo, Revisiting the preparation progress of nano-structured Si anodes toward industrial application from the perspective of cost and scalability, Adv. Energy Mater. 12 (7) (2022), 2102181.
[9] Xu Chen, Qinsong Bi, Muhammad Sajjad, Xu Wang, Yang Ren, Xiaowei Zhou, Wen Xu, Liu Zhu, One-dimensional porous silicon nanowires with large surface area for fast charge-discharge lithium-ion batteries, Nanomaterials 8 (5) (2018) 285.

[10] Jie Zhang, Sheng Fang, Xiaopeng Qi, Zhanglong Yu, Zhaohui Wu, Juanyu Yang, Shigang Lu, Preparation of high-purity straight silicon nanowires by molten salt electrolysis, J. Energy Chem. 40 (2020) 171–179.
[11] B. Gao, S. Sinha, L. Fleming, O. Zhou, Alloy Formation in nanostructured silicon, Adv. Mater. 13 (2001) 816.
[12] J. Graetz, C.C. Ahn, R. Yazami, B. Fultz, Highly reversible lithium storage in nanostructured silicon, Electrochem. Solid State Lett. 6 (2003) A194.
[13] Thomas M. Higgins, Sang-Hoon Park, Paul J. King, Chuanfang (John) Zhang, Niall McEvoy, Nina C. Berner, Dermot Daly, Aleksey Shmeliov, Umar Khan, Georg Duesberg, Valeria Nicolosi, Jonathan N. Coleman, A commercial conducting polymer as both binder and conductive additive for silicon nanoparticle-based lithium-ion battery negative electrodes, ACS Nano 10 (3) (2016) 3702–3713.
[14] Jeffrey Lopez, David G. Mackanic, Yi Cui, Zhenan Bao, Designing polymers for advanced battery chemistries, Nat. Rev. Mater. 4 (2019) 312–330.
[15] H. Wang, B. Wu, X. Wu, Q. Zhuang, T. Liu, Y. Pan, G. Shi, H. Yi, P. Xu, Z. Xiong, S.-L. Chou, B. Wang, Key factors for binders to enhance the electrochemical performance of silicon anodes through molecular design, Small 18 (2022), 2101680.
[16] W.-J. Zhang, A review of the electrochemical performance of alloy anodes for lithium-ion batteries, J. Power Sources 196 (2011) 13–24.
[17] X.H. Liu, H. Zheng, L. Zhong, S. Huang, K. Karki, L.Q. Zhang, Y. Liu, A. Kushima, W.T. Liang, J.W. Wang, et al., Anisotropic swelling and fracture of silicon nanowires during lithiation, Nano Lett. 11 (2011) 3312–3318.
[18] F. Tariq, V. Yufit, D.S. Eastwood, Y. Merla, M. Biton, B. Wu, Z. Chen, K. Freedman, G. Offer, E. Peled, et al., In-operando X-ray tomography study of lithiation induced delamination of Si based anodes for lithium-ion batteries, ECS Electrochem. Lett. 3 (2014) A76–A78.
[19] J.W. Choi, D. Aurbach, Promise and reality of post-lithium-ion batteries with high energy densities, Nat. Rev. Mater. 1 (2016), 16013.
[20] Andrea Miranda, Kasturi Sarang, Bolormaa Gendensuren, Eun-Suok Oh, Jodie Lutkenhaus, Rafael Verduzco, Molecular design principles for polymeric binders in silicon anodes, Mol. Syst. Des. Eng. 5 (2020) 709.
[21] Xiuyun Zhao, Svetlana Niketic, Chae-Ho Yim, Jigang Zhou, Jian Wang, Yaser Abu-Lebdeh, Revealing the role of poly(vinylidene fluoride) binder in Si/graphite composite anode for Li-ion batteries, ACS Omega 3 (9) (2018) 11684–11690.
[22] Hao Chen, Min Ling, Luke Hencz, Han Yeu Ling, Gaoran Li, Lin Zhan, Liu Gao, Shanqing Zhang, Exploring chemical, mechanical, and electrical functionalities of binders for advanced energy-storage devices, Chem. Rev. 118 (2018) 8936–8982.
[23] Qianyu Zhang, Chaofeng Zhang, Wenwei Luo, Lifeng Cui, Yan-Jie Wang, Tengyue Jian, Xiaolin Li, Qizhang Yan, Haodong Liu, Chuying Ouyang, Yulin Chen, Chun-Long Chen, Jiujun Zhang, Sequence-defined peptoids with -OH and -COOH groups as binders to reduce cracks of Si nanoparticles of lithium-ion batteries, Adv. Sci. 7 (2020), 2000749.
[24] N. Yuca, I. Kalafat, E. Guney, B. Cetin, O.S. Taskin, Self-healing systems in silicon anodes for Li-ion batteries, Materials 15 (2022) 2392.
[25] A.J. Fragoso-Medina, R.G. Escobedo-González, M.I. Nicolás-Vázquez, G.A. Arroyo-Razo, M.O. Noguez-Córdova, R. Miranda-Ruvalcaba, A DFT study of the geometrical, spectroscopical and reactivity properties of diindolylmethane-phenylboronic acid hybrids, Molecules 22 (10) (2017) 1744.
[26] E.C. Escudero-Adán, A. Bauzá, C. Lecomte, A. Frontera, Pablo Ballester, Boron triel bonding: a weak electrostatic interaction lacking electron-density descriptors, Phys. Chem. Chem. Phys. 20 (2018), 24192.
[27] S. Ossicini, O. Bisi, E. Degoli, I. Marri, F. Iori, E. Luppi, R. Magri, R. Poli, G. Cantele, D. Ninno, et al., First-principles study of silicon nanocrystals: structural and electronic properties, absorption, emission, and doping, J. Nanosci. Nanotechnol. 8 (2) (2008) 479–492.
[28] P. Giannozzi, Stefano Baroni, Nicola Bonini, Matteo Calandra, Roberto Car, Carlo Cavazzoni, Davide Ceresoli, Guido L. Chiarotti, Matteo Cococcioni, Ismaila Dabo, et al., Quantum ESPRESSO: a modular and open-source software project for quantum simulations of materials, J. Phys. Condens. Matter 21 (2009), 395502.
[29] D.R. Hamann, Optimized norm-conserving Vanderbilt pseudopotentials, Phys. Rev. B 88 (8) (2013).
[30] J.P. Perdew, K. Burke, M. Ernzerhof, Generalized gradient approximation made simple, Phys. Rev. Lett. 77 (1996) p3865–p3868.
[31] R. Fletcher, Practical Methods of Optimization, Wiley, New York, 1987.
[32] S. Grimme, Semiempirical GGA-type density functional constructed with a long-range dispersion correction, J. Comput. Chem. 27 (2006) 1787–1799.